

RESEARCH ARTICLE

Interspecific scaling of blood flow rates and arterial sizes in mammals

Roger S. Seymour^{1,*}, Qiaohui Hu¹, Edward P. Snelling^{2,3} and Craig R. White⁴

ABSTRACT

This meta-study investigated the relationships between blood flow rate (\dot{Q} ; $\text{cm}^3 \text{s}^{-1}$), wall shear stress (τ_w ; dyn cm^{-2}) and lumen radius (r_i ; cm) in 20 named systemic arteries of nine species of mammals, ranging in mass from 23 g mice to 652 kg cows, at rest. In the dataset, derived from 50 studies, lumen radius varied between 3.7 μm in a cremaster artery of a rat and 11.2 mm in the aorta of a human. The 92 logged data points of \dot{Q} and r_i are described by a single second-order polynomial curve with the equation: $\log \dot{Q} = -0.20 \log r_i^2 + 1.91 \log r_i + 1.82$. The slope of the curve increased from approximately 2 in the largest arteries to approximately 3 in the smallest ones. Thus, da Vinci's rule ($\dot{Q} \propto r_i^2$) applies to the main arteries and Murray's law ($\dot{Q} \propto r_i^3$) applies to the microcirculation. A subset of the data, comprising only cephalic arteries in which \dot{Q} is fairly constant, yielded the allometric power equation: $\dot{Q} = 155r_i^{2.49}$. These empirical equations allow calculation of resting perfusion rates from arterial lumen size alone, without reliance on theoretical models or assumptions on the scaling of wall shear stress in relation to body mass. As expected, \dot{Q} of individual named arteries is strongly affected by body mass; however, \dot{Q} of the common carotid artery from six species (mouse to horse) is also sensitive to differences in whole-body basal metabolic rate, independent of the effect of body mass.

KEY WORDS: Artery, Blood flow rate, Circulation, Da Vinci's rule, Murray's law, Wall shear stress

INTRODUCTION


The systemic arteries of mammals carry oxygenated blood to the tissues to support their aerobic metabolic demands. Therefore, there is a functional link between the size of the arteries, the rate of blood flow they transmit and the metabolic demand of the supplied tissues. Metabolic rate scales allometrically with body size, so there are likely to be patterns of cardiovascular variables that relate to body size in a functionally meaningful way. The empirical relationships between mammalian body size and heart mass, stroke volume, heart rate, cardiac output and blood pressure have each been shown to be related to metabolic rate, either directly or indirectly (Calder, 1996; Hillman and Hedrick, 2015; Seymour and Blaylock, 2000). The branching morphology of the arterial

system has been measured and modelled to test the optimality theory of a space-filling fractal network that supplies oxygenated blood with the least energy cost (Brummer et al., 2017; Hunt and Savage, 2016; Huo and Kassab, 2012, 2016; Kassab, 2006; Newberry et al., 2015; Price et al., 2007; Tekin et al., 2016). However, most of these studies focused only on the morphology of the network, and so it is difficult to extract the relationships between arterial size and actual blood flow rate. To address this limitation, the present study took an empirical approach by searching the literature and collecting paired measurements of arterial lumen radii and blood flow rates in 20 named systemic arteries of mammals. We hypothesized that the sizes of branching arteries should be related to the rate of blood flow within them, which depends directly on the absolute metabolic demand of the tissues and indirectly on body size.

Correlations between the metabolic rates of animals and the structure of supply networks are well known, but the direction of dependence is confusing in the literature. West, Brown and Enquist began a revolution in thinking about physiological scaling by suggesting that quarter-power scaling of metabolic rate and other traits should arise if vascular networks are selected to fill space while minimizing the energy required to distribute resources (Brummer et al., 2017; West et al., 1997). The vascular system has therefore been hypothesized to determine rates of metabolism (Newberry et al., 2015). An alternative perspective is that the allometric scaling of metabolic rate arises for reasons unrelated to the geometry of the vascular system (Kozłowski and Weiner, 1997). The need to deliver oxygen and nutrients to fuel rates of metabolism would then determine the structure of the vascular system. Distinguishing between the evolutionary explanations for the origin of metabolic scaling is challenging, but there are numerous examples demonstrating that metabolic demand determines the structure of the circulatory system. For example, the number and size of arteries are dynamically and reversibly adjusted throughout life to match the required rates of blood flow. Arteriogenesis (the increase in arterial diameter and wall thickness) and angiogenesis (the increase in the number of vessels by splitting or sprouting) occur in response to increases in metabolic demand of growing organs (Heil et al., 2006). The same phenomena occur in skeletal muscles during athletic training (Prior et al., 2004; Thijssen et al., 2012). Tumour metabolism becomes limited by perfusion during rapid growth, resulting in anaerobic metabolism and lactate that stimulates angiogenesis and subsequent oxygenation (Polet and Feron, 2013). Experimental changes in the blood flow regime of major arteries result in appropriate changes in diameter and wall thickness (Caro et al., 2012; Kamiya et al., 1984; Kamiya and Togawa, 1980; Langille, 1999; Smiesko and Johnson, 1993; Tronc et al., 1996; Wolinsky and Glagov, 1967). The success of coronary bypass surgery in which a vein is substituted for the diseased artery is due to the fact that the vein assumes a morphology similar to that of a healthy artery in a matter of weeks (Owens, 2010). It is clear that the

¹School of Biological Sciences, Faculty of Sciences, University of Adelaide, Adelaide, SA 5005, Australia. ²Department of Anatomy and Physiology, Faculty of Veterinary Science, University of Pretoria, Onderstepoort, Gauteng 0110, South Africa. ³Brain Function Research Group, School of Physiology, Faculty of Health Sciences, University of the Witwatersrand, Johannesburg, Gauteng 2193, South Africa. ⁴Centre for Geometric Biology, School of Biological Sciences, Faculty of Science, Monash University, Clayton, VIC 3800, Australia.

*Author for correspondence (roger.seymour@adelaide.edu.au)

 R.S.S., 0000-0002-3395-0059; Q.H., 0000-0003-3163-7859; E.P.S., 0000-0002-8985-8737; C.R.W., 0000-0002-0200-2187

List of symbols and abbreviations

BMR	basal metabolic rate (ml O ₂ h ⁻¹)
M _b	body mass (kg)
Q	volume blood flow rate (cm ³ s ⁻¹)
r _i	internal radius (cm)
η	blood viscosity (dyn s cm ⁻²)
τ _w	wall shear stress (dyn cm ⁻²)

morphology of the arteries is responsive to changes in metabolic demand, through changes in blood flow rate and blood pressure.

The physiological mechanisms responsible for controlling arterial size involve reversible interactions between blood flowing adjacent to the endothelium of the vessels and circumferential wall tension caused by blood pressure (Lu and Kassab, 2011). Higher blood flow rates over the glycocalyx of the endothelium initiate a series of responses involving inflammation, nitric oxide, vascular endothelial growth factor receptor proteins, metalloproteinases, cytokines and extracellular matrix proteins (Baeyens et al., 2015; Reitsma et al., 2007; Silvestre et al., 2013). The result is cellular proliferation in the vessel wall that enlarges the lumen and reduces blood velocity near the wall (Lehoux et al., 2006). Because the effects are reversible, they are thought to normalize wall shear stress (τ_w), which is an indirect measure of the stress on the glycocalyx of the endothelium. τ_w (dyn cm⁻²) can be measured directly as the derivative of the velocity gradient adjacent to the wall (Papaioannou and Stefanadis, 2005). τ_w can also be calculated from blood flow rate (\dot{Q} , cm³ s⁻¹), blood viscosity (η, dyn s cm⁻²) and arterial lumen radius (r_i, cm) according to the Poiseuille shear stress equation, $\tau_w = (4\dot{Q}\eta)/(\pi r_i^3)$, assuming that the flow conforms to the Poiseuille regime of a Newtonian fluid in a straight cylinder where the velocity profile is parabolic (Lehoux and Tedgui, 2003). However, the quantitative connection between the level of τ_w and the extent of vascular remodelling is obscure, because τ_w is either measured by the velocity gradient far from the wall or calculated from the shear stress equation without reference to the wall at all. Thus, the site of measurement in larger arteries is much farther from the wall than the very short (<5 μm) length of the glycocalyx (Reitsma et al., 2007).

Much of the twentieth century literature includes the idea that τ_w has a narrow 'set-point' range, typically ~10–20 dyn cm⁻², throughout the circulatory system (Glagov et al., 1988; Ku, 1997). However, Langille realized that τ_w in any particular artery is dependent on body mass (M_b; kg) (Langille, 1993). Based on his assumed scaling of cardiac output (∝M_b^{0.8}) and geometrically proportional scaling of arterial linear dimension (∝M_b^{0.33}), he calculated that aortic τ_w should scale allometrically with M_b^{-0.2}. More recently, data from mouse to human indicated that τ_w scales with M_b^{-0.38} for the infrarenal aorta (Greve et al., 2006; Weinberg and Ethier, 2007), M_b^{-0.23} for the common carotid artery (from fig. 2 in Cheng et al., 2007) and M_b^{-0.21} for the common carotid artery (from data in Weinberg and Ethier, 2007). For primates, τ_w appears to scale with M_b^{-0.20} for the internal carotid artery (Seymour et al., 2015) and M_b^{-0.22} for the vertebral artery (Boyer and Harrington, 2018a).

Few studies have considered the scaling of both the anatomy and the physiology of the cardiovascular system of mammals. In a now classic paper, Holt and colleagues (1981) measured the sizes of the main arteries and veins of seven species of mammals ranging in M_b from mice (~0.02 kg) to horses and cows (~500 kg) (Holt et al., 1981). The internal radius (r_i; cm) of the ascending aorta scaled with

M_b according to r_i=0.33M_b^{0.36}. The authors estimated the scaling of cardiac output to be proportional to M_b^{0.79} and, as radius scaled with M_b^{0.36}, radius squared (proportional to aortic cross-sectional area) scaled with M_b^{0.72}, and therefore the mean velocity of the blood scaled with M_b^{0.79-0.72}=M_b^{0.07}. Although the authors concluded that mean blood velocity is M_b independent, the exponent of 0.07 produces a doubling of velocity between mice and horses and cows. τ_w is also shown to decrease in the same artery of larger species; assuming that τ_w ∝ \dot{Q}/r^3 , then τ_w ∝ M_b^{0.79-(3×0.36)}=M_b^{-0.29}.

In the present study, we hypothesized that the negative scaling of τ_w with M_b is due to differences in the scaling of metabolic rate that would be reflected in the blood flow rates and the morphology of the arterial system. Rather than approaching the question from a theoretical model of fractal branching, we used an empirical approach to gather data from recent imaging studies of blood flow rate and arterial lumen size. This meta-study was designed to determine whether there are patterns of blood flow rate and τ_w in relation to *in vivo* arterial size among mammals over a wide range of M_b, and to determine whether blood flow rate is associated with whole-body basal metabolic rate, independent of M_b. The unexpected finding of our meta-study is that allometric equations can be used to estimate blood flow rate in mammalian arteries from their radius alone, without reference to theoretical equations or knowledge of τ_w, metabolic rate or M_b.

MATERIALS AND METHODS**Data collection**

Recent advancements in ultrasonic, X-ray and magnetic resonance imaging allowed us to collect data on systemic arterial radii and blood flow rates in mammals. The literature was searched for individual studies that included both pressurized internal radius and volume blood flow rate in the same arteries and the same species. All studies that presented data for both variables together were accepted and none were excluded. No record was made of the number of searched papers that failed to present data for both variables. However, because the literature was strongly biased toward studies on humans, followed by laboratory rodents, a deliberate effort was made to search for other species.

Arterial lumen size and volume blood flow rate were taken as reported means from control groups. In some instances, flow rate was calculated from mean velocity multiplied by cross-sectional lumen area. Arterial radius was calculated from either reported diameter or cross-sectional area, assuming the geometry of a perfect circle. τ_w was calculated from the Poiseuille shear stress equation, given in the Introduction, assuming a constant blood viscosity of 0.04 dyn s cm⁻² (Amin and Sirs, 1985; Schmid-Schönbein et al., 1969). There was good correlation between τ_w calculated this way and values reported in some individual studies that used the derivative of near-wall blood velocity gradients. Flow in a given artery was considered constant, laminar and Newtonian. Turbulent flow occurs only occasionally for the descending aorta or near a stenosis, valve or aneurysm (Winkel et al., 2015), so such conditions were excluded. Most animal studies involved some level of general anaesthesia or sedation, in which case the anaesthetic was recorded. Data from exercising animals were also recorded but excluded from the dataset because too few records were available. Body mass was taken from individual studies, either as a reported mean or as the average of a reported range. Missing M_b data were replaced with means from laboratory and domestic species (Jones et al., 2009; Seymour and Blaylock, 2000). Data for basal metabolic rate (BMR) were taken from a published compilation (Sieg et al., 2009) and supplemented with additional data for

horses (Eisenberg, 1981; Evans and Rose, 1988). BMR data for crab-eating macaques (*Macaca fascicularis*) were unavailable, so BMR data for similarly sized rhesus macaques (*Macaca mulatta*) were substituted.

Statistics

Values are presented as means with 95% confidence intervals (CI), calculated with Microsoft Excel add-in Statistix (www.statistix.com). Data for \dot{Q} , r_i , τ_w , M_b and BMR were \log_{10} -transformed for analysis. Polynomial or power regression equations were fitted with graphing and statistical software (GraphPad Software Inc., La Jolla, CA, USA). The relationships between \dot{Q} , M_b and BMR were analysed using linear mixed models with species identity as a random effect in lme4 v1.1-7 (<http://CRAN.R-project.org/package=lme4>) and lmerTest v2.0-25 (<http://CRAN.R-project.org/package=lmerTest>) packages of R v3.1.3 (<http://www.R-project.org/>). The significance of fixed effects was assessed using t -tests with Satterthwaite approximations to degrees of freedom and models fitted using maximum likelihood. One value for rats was excluded from this analysis because the individuals for which blood flow rate was determined were much smaller (100 g) than the individuals for which BMR was determined (290 g). For the remaining species, the $\log M_b$ of animals used for blood flow rate measurement were strongly correlated with the $\log M_b$ of animals used for metabolic rate measurement ($R^2=0.99$).

RESULTS

\dot{Q} and τ_w in relation to r_i

Data for arterial \dot{Q} and r_i were obtained from 50 studies that included both variables in the same paper and were measured from mammals at rest (see Table S1). The nine species comprised *Homo sapiens* and various domesticated or laboratory mammals. In total, there were 92 data points collected from 20 named systemic arteries. M_b

ranged from 23 g mice to 652 kg cows. r_i varied between 3.65 μm in a cremaster artery of a rat to 11.2 mm in the supraceliac aorta of a human. \dot{Q} ranged from 0.16 $\mu\text{m}^3 \text{s}^{-1}$ in the cremaster artery in a rat to 20 $\text{cm}^3 \text{s}^{-1}$ in the femoral artery of a horse.

The entire dataset was described by a single second-order polynomial equation relating $\log \dot{Q}$ to $\log r_i$: $\log \dot{Q} = -0.20 \log r_i^2 + 1.91 \log r_i + 1.82$ ($R^2=0.97$; $n=92$) (Fig. 1). The derivative (slope of the line at any point) of this equation revealed a gradual increase in slope with decreasing arterial size, from approximately 2 in the largest arteries to approximately 3 in the smallest ones.

τ_w is normally calculated according to the assumption of laminar flow with the Poiseuille shear stress equation, given in the Introduction. The data show increasing τ_w from 1.1 dyn cm^{-2} in the infrarenal aorta of humans to 163 dyn cm^{-2} in the small cremaster artery of the rat (Fig. 2). A polynomial equation was set to the data: $\log \tau_w = -0.20 \log r_i^2 - 1.09 \log r_i + 0.53$ ($R^2=0.62$; $n=92$).

\dot{Q} in the cephalic arteries only

A subset of the data was selected to include only the major cephalic arteries, because the blood flow regimes in these vessels are relatively constant (Fig. 3). These include the common carotid, internal carotid, vertebral, basilar, anterior cerebral, middle cerebral and posterior cerebral arteries. An allometric power regression was set to these data yielding the equation: $\dot{Q} = 155 r_i^{2.49 \pm 0.17}$ ($R^2=0.94$; $n=57$). The exponent was midway between 2 and 3 of the entire dataset.

Effect of M_b on \dot{Q} and τ_w in the femoral artery, aorta and common carotid artery

Three major arteries provided sufficient data to relate resting \dot{Q} to M_b allometrically (Fig. 4). The exponents were 0.80 for the femoral artery, 0.74 for the aorta and 0.80 for the common carotid artery. τ_w calculated for these arteries yielded exponents of -0.49 for the

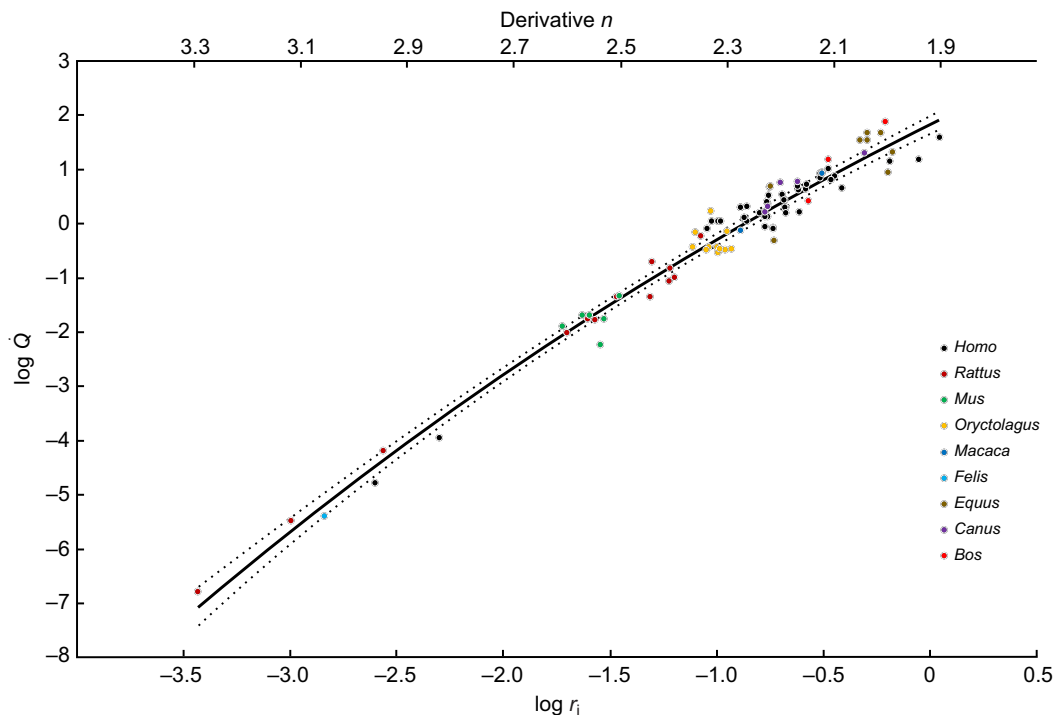


Fig. 1. Blood flow rates in mammalian arteries of different sizes. Relationship between \log blood flow rate (\dot{Q} ; $\text{cm}^3 \text{s}^{-1}$) and \log systemic arterial lumen radius (r_i ; cm) in nine genera of mammals at rest. The equation for the polynomial regression line is: $\log \dot{Q} = -0.20 \log r_i^2 + 1.91 \log r_i + 1.82$; 95% confidence bands for the regression line are shown. The value of the slope of the line at any point (derivative n) is given on the top axis.

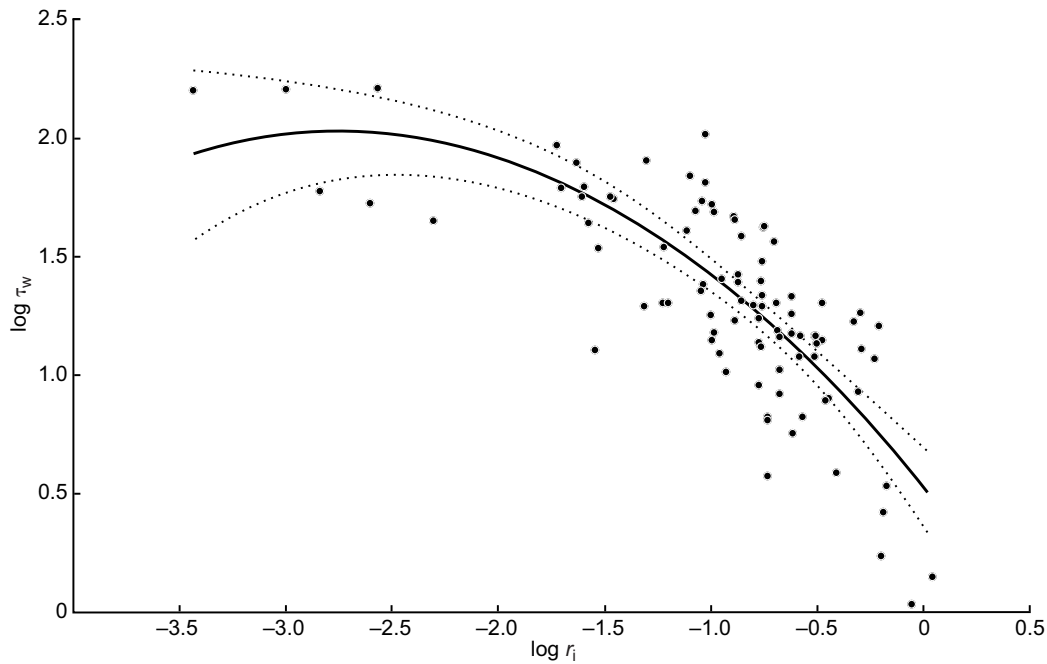


Fig. 2. Wall shear stress in mammalian arteries of different sizes. Relationship between log wall shear stress (τ_w ; dyn cm^{-2}) and log systemic arterial lumen radius (r_i ; cm) in mammals at rest, calculated from the Poiseuille shear stress equation: $\tau_w = (4\dot{Q}\eta)/(\pi r_i^3)$. The equation for the polynomial mean regression line is: $\log \tau_w = -0.20 \log r_i^2 - 1.09 \log r_i + 0.53$; 95% confidence bands for the regression line are shown.

femoral artery, -0.44 for the aorta and -0.14 for the common carotid artery (Fig. 5). See legends to Figs 4 and 5 for complete equations.

Effect of BMR on \dot{Q} in the common carotid artery

For species in which data on common carotid artery \dot{Q} were available, we found that their whole-body BMR ($\text{ml O}_2 \text{ h}^{-1}$)

scaled as $6.09 M_b^{0.71 \pm 0.07}$. Common carotid artery \dot{Q} ($\text{cm}^3 \text{ s}^{-1}$) scaled as $0.24 M_b^{0.80 \pm 0.09}$ and as $0.000157 \text{BMR}^{1.11 \pm 0.09}$. The correlation between common carotid artery \dot{Q} and BMR remained positive and significant ($t_{11.6} = 3.49$, $P = 0.005$) (Fig. 6), after accounting for the effect of M_b on \dot{Q} , which was not significant in the model that included BMR ($t_{11.6} = -0.90$, $P = 0.38$);

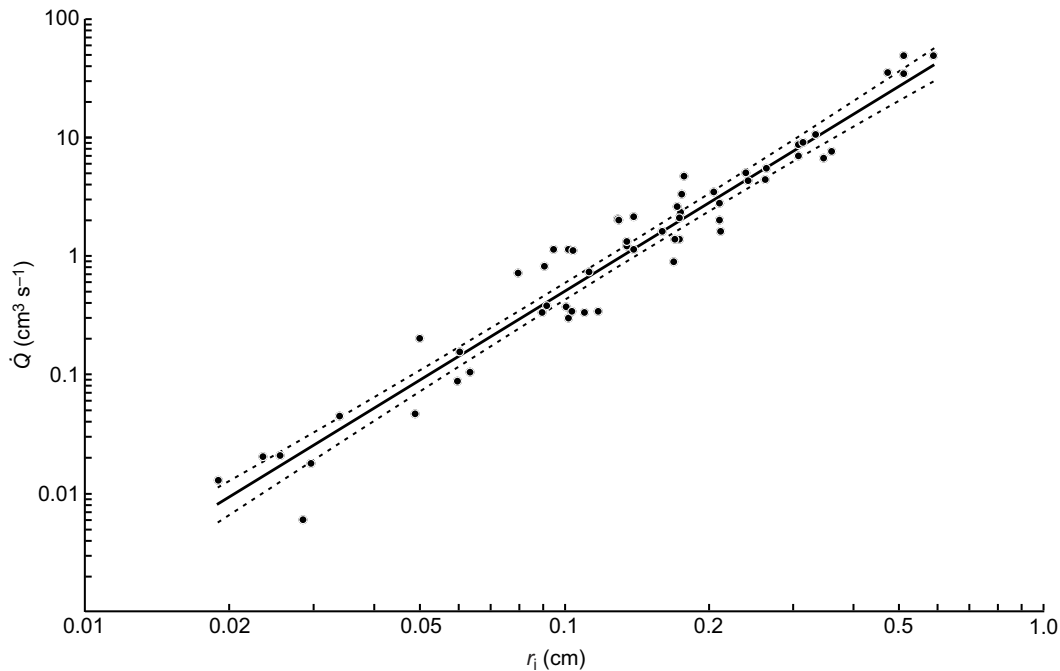


Fig. 3. Blood flow rates in cephalic arteries of different sizes. Subset of the data for blood flow rate (\dot{Q}) in relation to lumen radius (r_i) in the major cephalic arteries only, including the common carotid, internal carotid, vertebral, basilar, anterior cerebral, middle cerebral and posterior cerebral arteries for six genera of mammals (*Mus*, *Rattus*, *Oryctolagus*, *Canus*, *Homo*, *Equus*) at rest. The allometric equation for the power mean regression line of these arteries is: $\dot{Q} = 155 r_i^{2.49 \pm 0.17}$; 95% confidence bands for the regression line are shown. Note that arithmetic data are plotted on log axes.

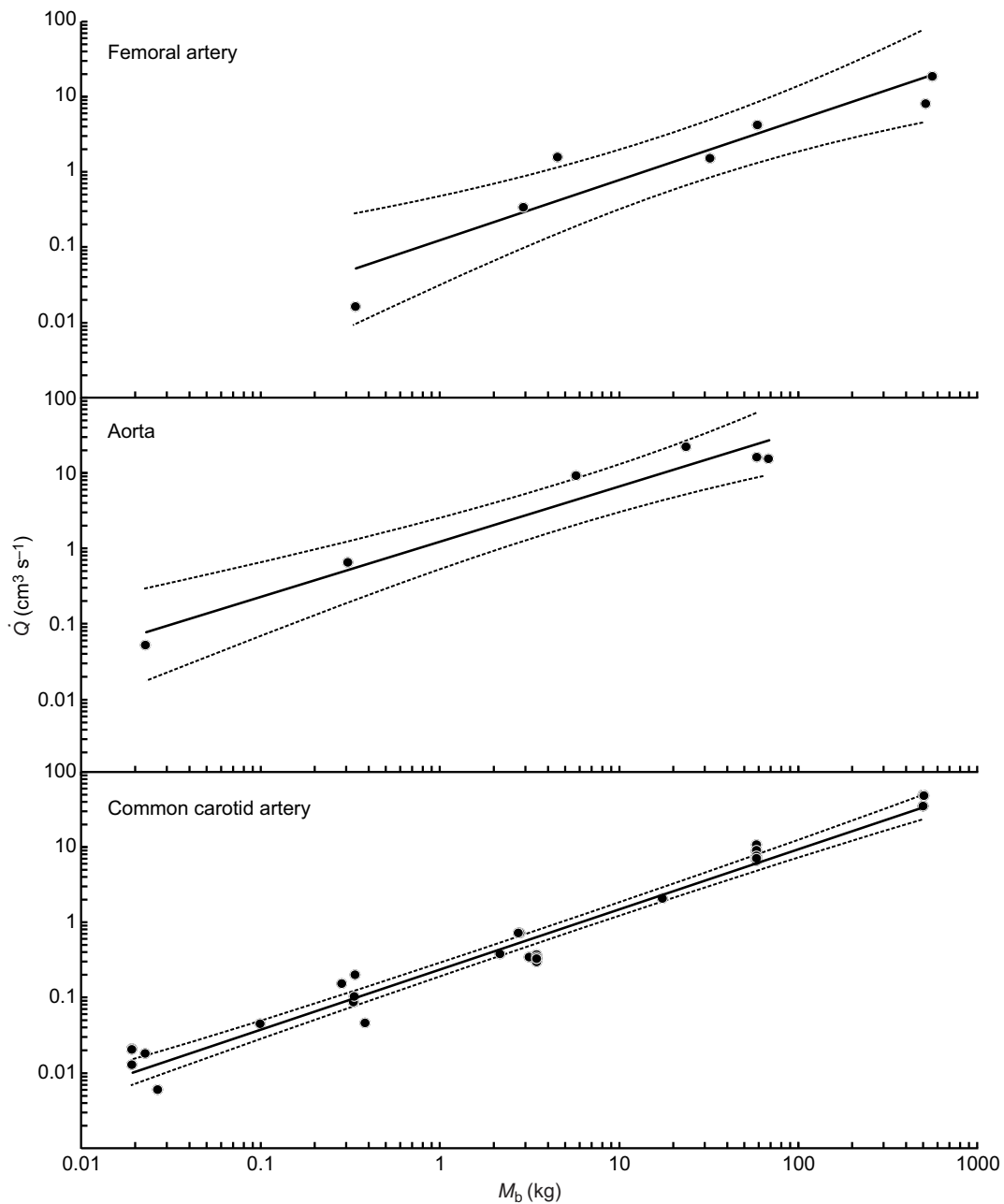


Fig. 4. Effect of body mass (M_b) on blood flow rate (\dot{Q}) in three major arteries of mammals at rest. The allometric equations are: femoral artery, $\dot{Q} = 0.12M_b^{0.80 \pm 0.34}$ ($R^2 = 0.88$; $n = 7$); aorta, $\dot{Q} = 1.15M_b^{0.74 \pm 0.24}$ ($R^2 = 0.95$; $n = 6$); common carotid artery, $\dot{Q} = 0.24M_b^{0.80 \pm 0.06}$ ($R^2 = 0.97$; $n = 31$); 95% confidence bands for each regression line are shown. Note that arithmetic data are plotted on log axes.

$\log \dot{Q} = -4.90 + 1.49 \log \text{BMR} - 0.279 \log M_b$. The effect of whole-body BMR on common carotid artery \dot{Q} remained significant ($t_{30} = 3.60$, $P = 0.001$) in a model that included vessel r_i ($t_{30} = 2.14$, $P = 0.04$) and M_b ($t_{30} = -1.53$, $P = 0.14$): $\log \dot{Q} = -3.02 + 1.23 \log \text{BMR} + 1.03 \log r_i - 0.411 \log M_b$.

DISCUSSION

\dot{Q} and r_i in resting mammals

The data gathered from 20 different systemic arteries in nine species of mammals differing in M_b by 4.5 orders of magnitude fell remarkably along a single, second-order polynomial regression line (Fig. 1). This close relationship is not simply a result of the influence of M_b . Although M_b is related to the size of individual named

arteries, the six smallest arteries in the dataset include those from rats, cats and humans, which differ greatly in M_b . The relationship between \dot{Q} and r_i is curved, with the derivative decreasing from a slope of approximately 2 in the largest arteries to about 3 in the smallest ones. The pattern is also apparent in different-sized arteries from humans and rats (Fig. 1). The explanation for this phenomenon was sought in the following theoretical models.

The circulatory system was analysed as a fractal-like branching network. Although the distal arteries appear to be close to geometrically dichotomously self-similar at every level (Family et al., 1989), the proximal arteries are not fractal, branching is not uniform and arterial anastomoses occur (Huo and Kassab, 2016). There are two classical models for anatomical branching pattern of

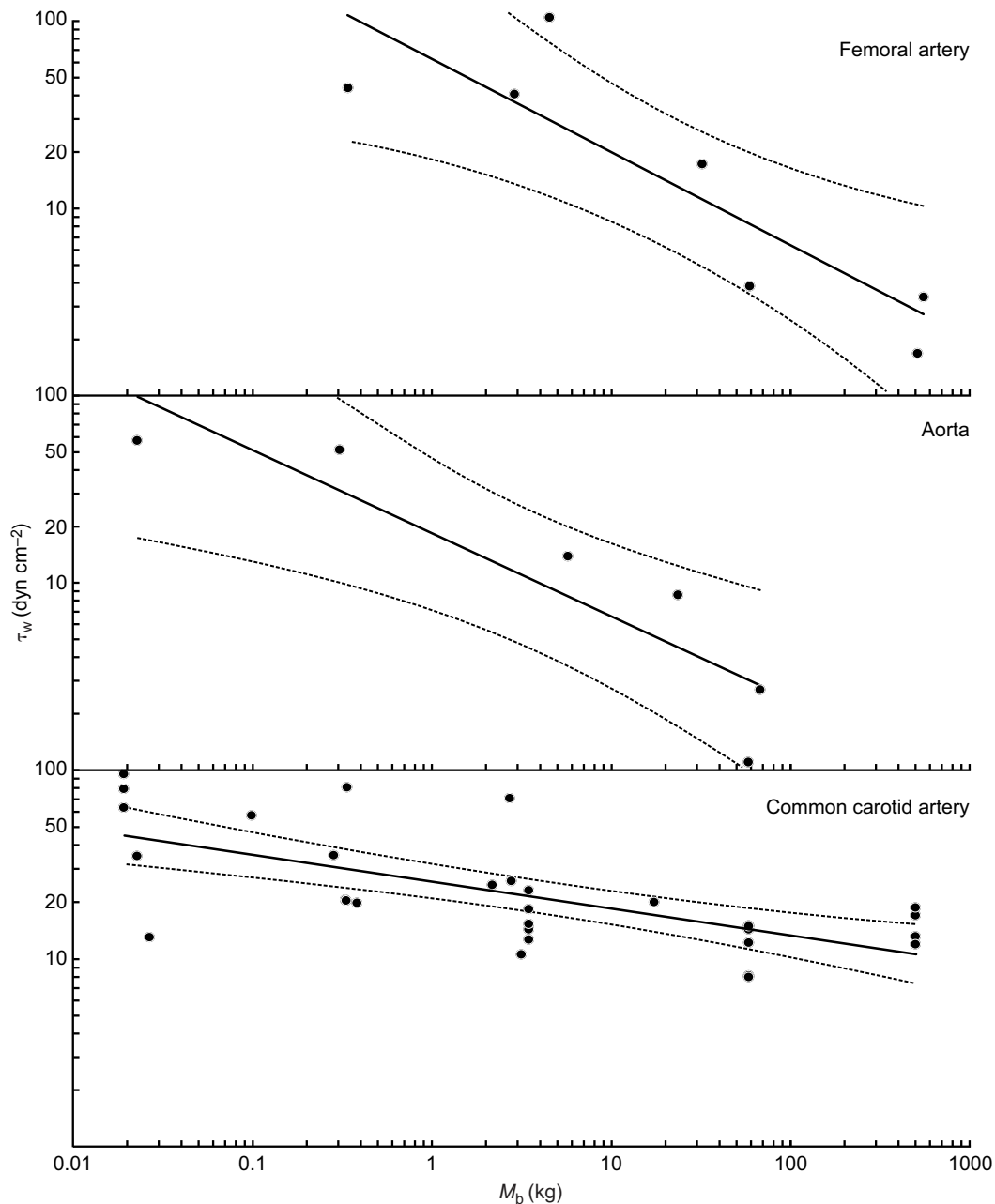


Fig. 5. Effect of body mass (M_b) on wall shear stress (τ_w) in three major arteries of mammals at rest. The allometric equations are: femoral artery, $\tau_w = 61M_b^{0.49 \pm 0.32}$ ($R^2 = 0.76$; $n = 6$); aorta, $\tau_w = 18M_b^{-0.44 \pm 0.29}$ ($R^2 = 0.82$; $n = 7$); common carotid artery, $\tau_w = 25M_b^{-0.14 \pm 0.06}$ ($R^2 = 0.45$; $n = 31$); 95% confidence bands for each regression line are shown. Note that arithmetic data are plotted on log axes.

the arterial tree. The first is the minimum energy loss hypothesis known as Murray's law, which predicts that $\dot{Q} \propto r^3$, such that r^3 of a parent artery is equal to the sum of r^3 of two daughter arteries (Murray, 1926). The other model, known as da Vinci's rule because the anatomist and artist Leonardo da Vinci recorded that the cross-sectional area of a parent artery is equal to the combined areas of the daughter arteries (Richter, 1970), predicts that $\dot{Q} \propto r^2$ (Zamir et al., 1992). Both are cases of the common relationship $r_p^n = r_{d1}^n + r_{d2}^n$, where r_p is the radius of the parent artery and r_{d1} and r_{d2} are the radii of the two daughter arteries. The exponent, n , is 3 for Murray's law and 2 for da Vinci's rule.

The present study shows that neither model holds for the entire arterial system. Rather, Murray's law applies to the smaller arteries,

as the derivative of the regression is close to 3, but da Vinci's rule applies to the larger arteries, where the derivative is approximately 2. These results confirm other indications from the literature. For example, among small arteries, $\dot{Q} \propto r^{2.76}$ in human retinal arteries (Riva et al., 1985), similar to retinal arteries of rhesus monkeys (Zamir and Medeiros, 1982), $\dot{Q} \propto r^{3.01}$ in the cremaster muscle arteries of rats (Mayrovitz and Roy, 1983) and $\dot{Q} \propto r^{2.98}$ in pial arteries on the surface of the brain of cats (Kobari et al., 1984).

For the larger arteries, several studies conclude that \dot{Q} should be proportional to radius squared. A meta-study of five species of mammals indicated that τ_w is related to arterial diameter to the -0.50 power, which indicates that $\dot{Q} \propto r^{2.5}$ (Cheng et al., 2007). Zamir et al. (1992) measured diameters in casts made from human

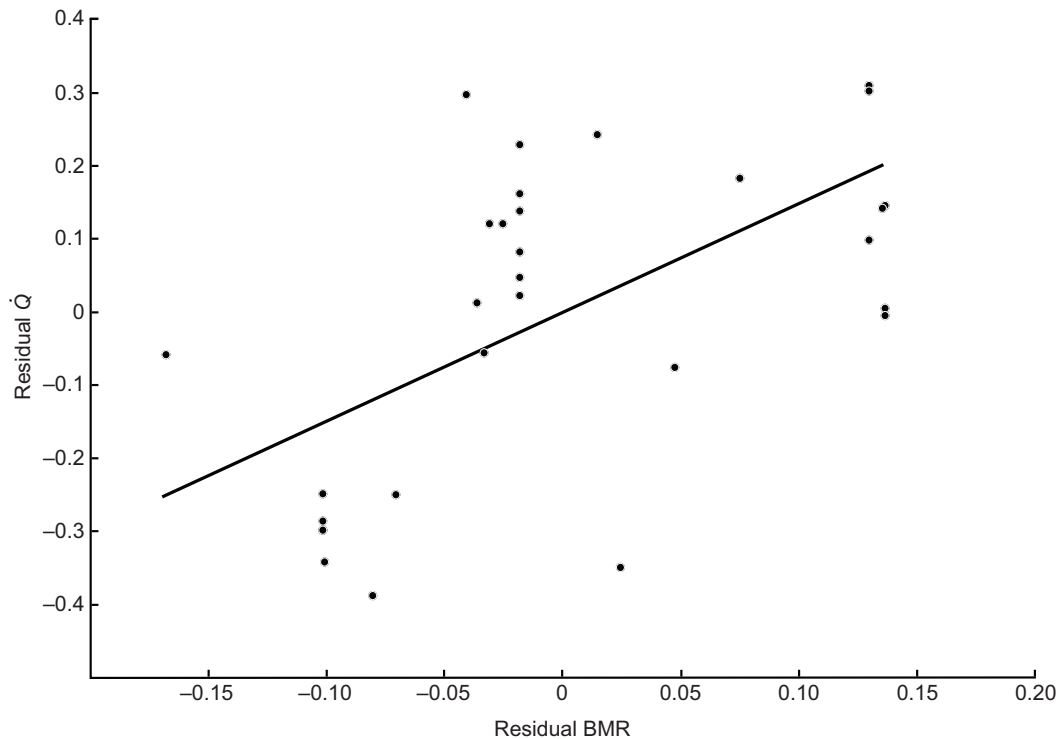


Fig. 6. Influence of basal metabolic rate on arterial blood flow rate. Relationship between the residuals of log common carotid artery blood flow rate (\dot{Q} , $\text{cm}^3 \text{s}^{-1}$) and the residuals of log whole-body basal metabolic rate (BMR, $\text{ml O}_2 \text{h}^{-1}$). Because both variables are significantly related to body mass (M_b , kg), residuals of each variable from linear regressions that relate \dot{Q} and BMR to M_b are shown. The line represents the parameter estimate for the effect of BMR on \dot{Q} , accounting for M_b , in a linear mixed model including a random effect of species identity: $\log \dot{Q} = -4.90 + 1.49 \log \text{BMR} - 0.279 \log M_b$.

central arteries and found that n is closer to 2 than 3. An intraspecific analysis of all major arteries with 3–10 branch levels in the human head and torso revealed high variability, but a mean empirical exponent equivalent to 2.04 or 2.44, depending on the estimation model employed (Newberry et al., 2015). The exponents for arterial size of vascular trees in organs of humans and laboratory animals range widely, approximately from 2 to 4 (Kassab, 2006). An alternative model to Murray's law, but also based on fractal-like branching of the arterial tree with minimal energy loss, concludes that the exponent is between 2 and 3 (Huo and Kassab, 2016).

The shift from da Vinci's rule in larger arteries to Murray's law in smaller ones has been explained in theoretical studies (Savage et al., 2008; West et al., 1997, 1999). The area-preserving relationship of da Vinci's rule (where exponent $n=2$) ensures that energy loss by reflected pressure waves is minimized in the major arteries (Gafiychuk and Lubashevsky, 2001). If the mean velocity in the parent is equal to the mean velocity in the daughters, and the wall characteristics are the same in the parent and daughters, then changes in velocity at the junction are not converted to reflected waves (Caro et al., 2012). Murray's law (where exponent $n=3$) minimizes friction-related energy loss, because wall shear stress is equal in parent and daughter arteries, and permits the velocity of the blood to slow down at the level of the capillaries to allow sufficient time for gas exchange.

Scaling of \dot{Q} and r_i in the cephalic arteries only

The entire dataset contains arteries that service tissues of varying metabolic rate. In particular, the inferior aorta, femoral arteries and brachial arteries largely supply skeletal muscles, while the common carotid and vertebral arteries and their branches mainly supply the

brain. Flow regimes in these two categories are vastly different. For instance, \dot{Q} in the femoral artery can increase 10-fold between rest and activity (Jorfeldt and Wahren, 1971). Therefore, the diameter of the femoral artery is matched better with maximum \dot{Q} than resting \dot{Q} . In contrast to muscle perfusion, brain perfusion is autoregulated and relatively constant globally, although there may be regional redistribution of blood (Ogoh and Ainslie, 2009; Payne, 2016). For example, \dot{Q} in the common carotid artery of humans is independent of heart rate (Wilcox et al., 1970). During moderate, steady-state cycling exercise that causes a doubling of cardiac output, global cerebral \dot{Q} increases only 28% above resting rates after 3 min and returns to resting rates after a further 13 min of exercise (Hiura et al., 2014). \dot{Q} in the middle cerebral and internal carotid arteries increases by only 14% and 17%, respectively, despite doubling of heart rate during moderate cycling exercise (at 60–67% of maximal aerobic capacity), and the increase in \dot{Q} along these arteries is even less during more intense cycling exercise (80–90% of maximal aerobic capacity) (Hellström et al., 1996). In a similar experiment, Japanese women increased cardiac output by 260% during moderate cycling exercise, but increased internal carotid arterial \dot{Q} by only 18% and vertebral artery \dot{Q} by 33% (Sato and Sadamoto, 2010). The diameters of the cerebral arteries also change very little between rest and activity (Hellström et al., 1996) or in response to changes in blood pressure and blood gas levels (Payne, 2016). There is also almost no difference in cerebral \dot{Q} when humans engage in mental arithmetic (Sokoloff et al., 1955) or between awake and sleeping states (Townsend et al., 1973). Cerebral \dot{Q} of humans decreases gradually with age in absolute terms, but not when expressed relative to brain mass, despite rising arterial blood pressure (Meltzer et al., 2000; Tarumi and Zhang, 2018; van Es et al., 2010). However, cerebral \dot{Q} in humans is responsive to

short-term experimental alterations in mean arterial blood pressure (Tan, 2012; Willie et al., 2014), defending more strongly against increases in pressure than decreases (Numan et al., 2014).

The relationship between \dot{Q} and r_i in the cephalic arteries was best described by an allometric power equation (Fig. 3). The relationship was determined mainly by the data for the common carotid arteries from a 27 g mouse to a 500 kg horse. The exponent of the equation was 2.49 and the 95% CI of the exponent was 0.17. Thus, the exponent lies midway between, but is significantly different from, those expected for da Vinci's rule (where $n=2$) and Murray's law (where $n=3$).

τ_w in relation to r_i and M_b

The general trend in this meta-study indicates that τ_w increases as blood passes into progressively smaller arteries (Fig. 2), in contrast to a generally assumed independence of τ_w from vessel size and M_b according to Murray's law. Thus, our results from 50 studies of nine species of mammals confirm the pattern from seven studies of five species of mammals, which showed that τ_w in the common carotid artery increases from approximately 11 to 65 dyn cm⁻² from humans to mice (Cheng et al., 2007). Our data indicate an increase from 14 to 42 dyn cm⁻² over the same M_b range.

\dot{Q} in three major arteries scaled with M_b with exponents between 0.74 and 0.80 (Fig. 4), which is consistent with the scaling of cardiac output in resting mammals, ca. 0.80 (Calder, 1996; Holt et al., 1981). Calculated τ_w in these arteries decreased with increasing M_b , with large negative exponents in the femoral artery (-0.49) and aorta (-0.44), but a smaller negative exponent in the common carotid artery (-0.14) (Fig. 5). By comparison, the exponent was reported to be -0.38 in the aorta (Greve et al., 2006; Weinberg and Ethier, 2007) and between -0.20 and -0.23 in the common carotid, internal carotid and vertebral arteries (Boyer and Harrington, 2018a; Cheng et al., 2007; Greve et al., 2006; Seymour et al., 2015; Weinberg and Ethier, 2007). This may represent a decreased sensitivity of τ_w to body size in arteries that supply mainly nervous tissue as opposed to arteries that supply a large fraction of blood to muscles during activity, but are measured at rest. In fact, τ_w is quite low in the femoral artery at rest, but increases during activity to be comparable to that in the similarly sized common carotid artery at rest (Kornet et al., 2000).

The standard shear stress equation assumes that τ_w is inversely proportional to r_i^3 . If \dot{Q} is also proportional to r_i^3 , then τ_w is a constant (i.e. $\tau_w \propto r_i^0$). If \dot{Q} is proportional to r_i^2 , then τ_w should increase in smaller arteries ($\tau_w \propto r_i^{-1}$), which appears to be the case (Fig. 2). However, we found that the exponent in fact varies between 3 and 2 depending on arterial size, so we can calculate τ_w according to a modified shear stress equation, $\tau_w = (4\dot{Q}\eta)/(\pi r_i^n)$, where n is the derivative of the polynomial equation for \dot{Q} and r_i . The descriptive equation for the curve based on the derivative is $\log \tau_w = 0.200 \log r_i^2 - 0.017 \log r_i + 0.530$ ($R^2 = 0.70$; $n = 92$) (Fig. S1). This modified equation also shows that τ_w increases with decreasing arterial size, from nearly 3 dyn cm⁻² in the largest arteries to above 1500 dyn cm⁻² in the cremaster arteries of rats, which is certainly unrealistically high. All of the calculations of τ_w should be approached with caution for three reasons. First, the standard equation assumes that τ_w is inversely proportional to r_i^3 , which is doubtful. Second, they are based on flow rates during rest, but flow rates in large arteries supplying muscles can increase greatly, without a complete compensatory increase in radius (Cheng et al., 2003). Third, they assume that blood viscosity is constant, but the effective viscosity near the wall of the smallest arteries might be reduced (Sriram et al., 2014).

\dot{Q} in relation to BMR

The most represented artery in the dataset was the common carotid artery. When the effect of M_b was accounted for, there was a positive relationship between common carotid artery \dot{Q} and whole-body BMR (Fig. 6). This implies that species with higher BMR also have higher cephalic perfusion rates and brain metabolic rates. This positive relationship is similar to the relationship observed between brain size and metabolic rate in several studies of eutherian mammals. M_b -independent brain size is positively correlated with M_b -independent metabolic rate in humans (Javed et al., 2010; Müller et al., 2011) and inbred strains of mice (Konarzewski and Diamond, 1995), and in eutherian mammals in general (Navarrete et al., 2011; Weisbecker and Goswami, 2010). In contrast, there is no relationship between brain size and metabolic rate in marsupials (Weisbecker and Goswami, 2010), birds (Isler and van Schaik, 2006) or teleost fishes (Killen et al., 2016).

The correlation between brain size and metabolic rate, where present, and the correlation between common carotid artery blood flow rate and whole-body BMR may arise because the brain is energetically expensive to maintain and contributes significantly to whole-body metabolism. The human brain is certainly expensive, accounting for around 20% of BMR, but the contribution is much smaller (2–8%) in most non-primate species (Mink et al., 1981), although there are some notable exceptions (Nilsson, 1996). The proximate cause of the relationship between M_b -independent BMR and M_b -independent brain size has long been controversial (McNab and Eisenberg, 1989). It may arise indirectly via extrinsic factors that influence both brain size and metabolic rate, rather than directly as a functional consequence of the contribution of the brain to whole-body metabolism (Glazier, 2018; McNab and Köhler, 2017; White and Kearney, 2013). It is possible that mammals with high BMR are generally more active and require a greater ability to process sensory information quickly.

Practical use of the equations

If the size of the lumen of an artery subject to normal physiological blood pressures is known, \dot{Q} can be estimated. The second-order polynomial equation for the entire dataset (Fig. 1) is useful over the broad range of vessel size and can be applied loosely to any mammal, even if the destination of the arterial blood (e.g. neural or muscular) is not known. Because \dot{Q} in the cephalic arteries is rather constant, the power equation (Fig. 3) can be used more precisely to estimate \dot{Q} to the brain. The usefulness of the equations is enhanced over previous attempts, because they do not involve adherence to theory ($\dot{Q} \propto r_i^3$) and there are no assumptions about the scaling of τ_w on M_b . In particular, we previously used the relationship $\dot{Q} = (\tau_w \pi r_i^3)/(4\eta)$ and assumed that $\tau_w = 167M_b^{0.20}$, based on data from only humans and rats, to estimate \dot{Q} through the internal carotid artery from the radius of the carotid foramen (Seymour et al., 2015). This assumption was tenuous, not only because it was based on just two species but also because the functional relationship between τ_w and M_b was quite obscure. This aspect of our method was criticized (Boyer and Harrington, 2018a), defended (Seymour and Snelling, 2018) and then supported (Boyer and Harrington, 2018b). With the present analysis, however, we can circumvent the issue altogether and not involve τ_w or M_b . The new empirical equations apply well to a broad range of arteries over a broad range of body size under resting conditions, so they offer the prospect of estimating blood flow rate (and hence oxygen delivery and metabolic rate) in organs according to the size of their supply arteries.

Acknowledgements

We acknowledge two anonymous reviewers for their valuable suggestions and corrections of the first submission.

Competing interests

The authors declare no competing or financial interests.

Author contributions

Conceptualization: R.S.S.; Methodology: R.S.S., Q.H., C.R.W.; Software: C.R.W.; Formal analysis: R.S.S., Q.H., E.P.S., C.R.W.; Resources: R.S.S.; Data curation: R.S.S.; Writing - original draft: R.S.S.; Writing - review & editing: R.S.S., Q.H., E.P.S., C.R.W.; Project administration: R.S.S.; Funding acquisition: R.S.S.

Funding

The research was supported by the Australian Research Council (Project 'Design of the cardiovascular system of living and fossil vertebrates', grant DP 170104952).

Supplementary information

Supplementary information available online at <http://jeb.biologists.org/lookup/doi/10.1242/jeb.199554.supplemental>

References

- Amin, T. M. and Sirs, J. A. (1985). The blood rheology of man and various animal species. *Q. J. Exp. Physiol. Cognate Med. Sci.* **70**, 37-49.
- Baeyens, N., Nicolli, S., Coon, B. G., Ross, T. D., Van den Dries, K., Han, J., Lauridsen, H. M., Mejean, C. O., Eichmann, A., Thomas, J.-L. et al. (2015). Vascular remodeling is governed by a VEGFR3-dependent fluid shear stress set point. *eLife* **4**, e04645.
- Boyer, D. M. and Harrington, A. R. (2018a). Scaling of bony canals for encephalic vessels in euarchontans: implications for the role of the vertebral artery and brain metabolism. *J. Hum. Evol.* **114**, 85-101.
- Boyer, D. M. and Harrington, A. R. (2018b). New estimates of blood flow rates in the vertebral artery of euarchontans and their implications for encephalic blood flow scaling: a response to Seymour and Snelling (2018). *J. Hum. Evol.* **128**, 93-98.
- Brummer, A. B., Savage, V. M. and Enquist, B. J. (2017). A general model for metabolic scaling in self-similar asymmetric networks. *PLoS Comput. Biol.* **13**, e1005394.
- Calder, W. A., III. (1996). *Size, Function, and Life History*. Mineola, New York: Dover Publications.
- Caro, C. G., Pedley, T. J., Schroter, R. C. and Seed, W. A. (2012). *The Mechanics of the Circulation*. Cambridge: Cambridge University Press.
- Cheng, C. P., Herfkens, R. J. and Taylor, C. A. (2003). Abdominal aortic hemodynamic conditions in healthy subjects aged 50-70 at rest and during lower limb exercise: *in vivo* quantification using MRI. *Atherosclerosis* **168**, 323-331.
- Cheng, C., Helderma, F., Tempel, D., Segers, D., Hierck, B., Poelmann, R., van Tol, A., Duncker, D. J., Robbers-Visser, D., Ursem, N. T. C. et al. (2007). Large variations in absolute wall shear stress levels within one species and between species. *Atherosclerosis* **195**, 225-235.
- Eisenberg, J. F. (1981). *The Mammalian Radiations: An Analysis of Trends in Evolution, Adaptation, and Behavior*. Chicago: University of Chicago Press.
- Evans, D. L. and Rose, R. J. (1988). Dynamics of cardiorespiratory function in standardbred horses during different intensities of constant-load exercise. *J. Comp. Physiol. B* **157**, 791-799.
- Family, F., Masters, B. R. and Platt, D. E. (1989). Fractal pattern formation in human retinal vessels. *Physica D* **38**, 98-103.
- Gafiychuk, V. V. and Lubashevsky, I. A. (2001). On the principles of the vascular network branching. *J. Theor. Biol.* **212**, 1-9.
- Glagov, S., Zarins, C., Giddens, D. P. and Ku, D. N. (1988). Hemodynamics and atherosclerosis - insights and perspectives gained from studies of human arteries. *Arch. Pathol. Lab. Med.* **112**, 1018-1031.
- Glazier, D. S. (2018). Rediscovering and reviving old observations and explanations of metabolic scaling in living systems. *Systems* **6**, e6010004.
- Greve, J. M., Les, A. S., Tang, B. T., Blomme, M. T. D., Wilson, N. M., Dalman, R. L., Pelc, N. J. and Taylor, C. A. (2006). Allometric scaling of wall shear stress from mice to humans: quantification using cine phase-contrast MRI and computational fluid dynamics. *Am. J. Physiol. Heart Circ. Physiol.* **291**, H1700-H1708.
- Heil, M., Eitenmüller, I., Schmitz-Rixen, T. and Schaper, W. (2006). Arteriogenesis versus angiogenesis: similarities and differences. *J. Cell. Mol. Med.* **10**, 45-55.
- Hellström, G., Fischer-Colbrie, W., Wahlgren, N. G. and Jogestrand, T. (1996). Carotid artery blood flow and middle cerebral artery blood flow velocity during physical exercise. *J. Appl. Physiol.* **81**, 413-418.
- Hillman, S. S. and Hedrick, M. S. (2015). A meta-analysis of *in vivo* vertebrate cardiac performance: implications for cardiovascular support in the evolution of endothermy. *J. Exp. Biol.* **218**, 1143-1150.
- Hiura, M., Nariai, T., Ishii, K., Sakata, M., Oda, K., Toyohara, J. and Ishiwata, K. (2014). Changes in cerebral blood flow during steady-state cycling exercise: a study using oxygen-15-labeled water with PET. *J. Cereb. Blood Flow Metab.* **34**, 389-396.
- Holt, J. P., Rhode, E. A., Holt, W. W. and Kines, H. (1981). Geometric similarity of aorta, venae cavae, and certain of their branches in mammals. *Am. J. Physiol. Regul. Integr. Comp. Physiol.* **241**, R100-R104.
- Hunt, D. and Savage, V. M. (2016). Asymmetries arising from the space-filling nature of vascular networks. *Phys. Rev. E* **93**, 062305.
- Huo, Y. and Kassab, G. S. (2012). Intraspecific scaling laws of vascular trees. *J. R. Soc. Interface* **9**, 190-200.
- Huo, Y. L. and Kassab, G. S. (2016). Scaling laws of coronary circulation in health and disease. *J. Biomech.* **49**, 2531-2539.
- Isler, K. and van Schaik, C. (2006). Costs of encephalization: the energy trade-off hypothesis tested on birds. *J. Hum. Evol.* **51**, 228-243.
- Javed, F., He, Q., Davidson, L. E., Thornton, J. C., Albu, J., Boxt, L., Krasnow, N., Elia, M., Kang, P., Heshka, S. et al. (2010). Brain and high metabolic rate organ mass: contributions to resting energy expenditure beyond fat-free mass. *Am. J. Clin. Nutr.* **91**, 907-912.
- Jones, K. E., Bielby, J., Cardillo, M., Fritz, S. A., O'Dell, J., Orme, C. D. L., Safi, K., Sechrest, W., Boakes, E. H., Carbone, C. et al. (2009). PanTHERIA: a species-level database of life history, ecology, and geography of extant and recently extinct mammals. *Ecology* **90**, 2648.
- Jorfeldt, L. and Wahren, J. (1971). Leg blood flow during exercise in man. *Clin. Sci.* **41**, 459-473.
- Kamiya, A. and Togawa, T. (1980). Adaptive regulation of wall shear stress to flow change in the canine carotid artery. *Am. J. Physiol. Heart Circ. Physiol.* **239**, H14-H21.
- Kamiya, A., Bukhari, R. and Togawa, T. (1984). Adaptive regulation of wall shear stress optimizing vascular tree function. *Bull. Math. Biol.* **46**, 127-137.
- Kassab, G. S. (2006). Scaling laws of vascular trees: of form and function. *Am. J. Physiol. Heart Circ. Physiol.* **290**, H894-H903.
- Killen, S. S., Glazier, D. S., Rezende, E. L., Clark, T. D., Atkinson, D., Willener, A. S. T. and Halsey, L. G. (2016). Ecological influences and morphological correlates of resting and maximal metabolic rates across teleost fish species. *Am. Nat.* **187**, 592-606.
- Kobari, M., Gotoh, F., Fukuuchi, Y., Tanaka, K., Suzuki, N. and Uematsu, D. (1984). Blood flow velocity in the pial arteries of cats, with particular reference to the vessel diameter. *J. Cereb. Blood Flow Metab.* **4**, 110-114.
- Konarzowski, M. and Diamond, J. (1995). Evolution of basal metabolic rate and organ masses in laboratory mice. *Evolution* **49**, 1239-1248.
- Kornet, L., Hoeks, A. P. G., Lambregts, J. and Reneman, R. S. (2000). Mean wall shear stress in the femoral arterial bifurcation is low and independent of age at rest. *J. Vasc. Res.* **37**, 112-122.
- Kozłowski, J. and Weiner, J. (1997). Interspecific allometries are by-products of body size optimization. *Am. Nat.* **149**, 352-380.
- Ku, D. N. (1997). Blood flow in arteries. *Annu. Rev. Fluid Mech.* **29**, 399-434.
- Langille, B. L. (1993). Remodeling of developing and mature arteries: endothelium, smooth-muscle, and matrix. *J. Cardiovasc. Pharmacol.* **21**, S11-S17.
- Langille, B. L. (1999). Fluid dynamics in vascular pathology: adaptations of the arterial wall to chronic changes in blood flow. *J. Vasc. Surg.* **29**, 1106-1108.
- Lehoux, S. and Tedgui, A. (2003). Cellular mechanics and gene expression in blood vessels. *J. Biomech.* **36**, 631-643.
- Lehoux, S., Castier, Y. and Tedgui, A. (2006). Molecular mechanisms of the vascular responses to haemodynamic forces. *J. Intern. Med.* **259**, 381-392.
- Lu, D. and Kassab, G. S. (2011). Role of shear stress and stretch in vascular mechanobiology. *J. R. Soc. Interface* **8**, 1379-1385.
- Mayrovitz, H. N. and Roy, J. (1983). Microvascular blood-flow: evidence indicating a cubic dependence on arteriolar diameter. *Am. J. Physiol. Heart Circ. Physiol.* **245**, 1031-1038.
- McNab, B. K. and Eisenberg, J. F. (1989). Brain size and its relation to the rate of metabolism in mammals. *Am. Nat.* **133**, 157-167.
- McNab, B. K. and Köhler, M. (2017). The difficulty with correlations: energy expenditure and brain mass in bats. *Comp. Biochem. Physiol. A Mol. Integr. Physiol.* **212**, 9-14.
- Meltzer, C. C., Cantwell, M. N., Greer, P. J., Ben-Eliezer, D., Smith, G., Frank, G., Kaye, W. H., Houck, P. R. and Price, J. C. (2000). Does cerebral blood flow decline in healthy aging? A PET study with partial-volume correction. *J. Nucl. Med.* **41**, 1842-1848.
- Mink, J. W., Blumenschine, R. J. and Adams, D. B. (1981). Ratio of central nervous system to body metabolism in vertebrates: its constancy and functional basis. *Am. J. Physiol. Regul. Integr. Comp. Physiol.* **241**, R203-R212.
- Müller, M. J., Langemann, D., Gehrke, I., Later, W., Heller, M., Glüer, C. C., Heymsfield, S. B. and Bosy-Westphal, A. (2011). Effect of constitution on mass of individual organs and their association with metabolic rate in humans—a detailed view on allometric scaling. *PLoS ONE* **6**, e22732.
- Murray, C. D. (1926). The physiological principle of minimum work. I. The vascular system and the cost of blood volume. *Proc. Natl. Acad. Sci. USA* **12**, 207-214.
- Navarrete, A., van Schaik, C. P. and Isler, K. (2011). Energetics and the evolution of human brain size. *Nature* **480**, 91-93.

- Newberry, M. G., Ennis, D. B. and Savage, V. M.** (2015). Testing foundations of biological scaling theory using automated measurements of vascular networks. *PLoS Comput. Biol.* **11**, e1004455.
- Nilsson, G. E.** (1996). Brain and body oxygen requirements of *Gnathonemus petersii*, a fish with an exceptionally large brain. *J. Exp. Biol.* **199**, 603-607.
- Numan, T., Bain, A. R., Hoiland, R. L., Smirl, J. D., Lewis, N. C. and Ainslie, P. N.** (2014). Static autoregulation in humans: a review and reanalysis. *Med. Eng. Phys.* **36**, 1487-1495.
- Ogoh, S. and Ainslie, P. N.** (2009). Cerebral blood flow during exercise: mechanisms of regulation. *J. Appl. Physiol.* **107**, 1370-1380.
- Owens, C. D.** (2010). Adaptive changes in autogenous vein grafts for arterial reconstruction: clinical implications. *J. Vasc. Surg.* **51**, 736-746.
- Papaioannou, T. G. and Stefanadis, C.** (2005). Vascular wall shear stress: basic principles and methods. *Hellenic J. Cardiol.* **46**, 9-15.
- Payne, S.** (2016). *Cerebral Autoregulation: Control of Blood Flow in the Brain*. Switzerland: Springer Nature.
- Polet, F. and Feron, O.** (2013). Endothelial cell metabolism and tumour angiogenesis: glucose and glutamine as essential fuels and lactate as the driving force. *J. Intern. Med.* **273**, 156-165.
- Price, C. A., Enquist, B. J. and Savage, V. M.** (2007). A general model for allometric covariation in botanical form and function. *Proc. Natl. Acad. Sci. USA* **104**, 13204-13209.
- Prior, B. M., Yang, H. T. and Terjung, R. L.** (2004). What makes vessels grow with exercise training? *J. Appl. Physiol.* **97**, 1119-1128.
- Reitsma, S., Slaaf, D. W., Vink, H., van Zandvoort, M. A. M. J. and oude Egbrink, M.** (2007). The endothelial glycocalyx: composition, functions, and visualization. *Pflugers Arch. Eur. J. Physiol.* **454**, 345-359.
- Richter, J. P.** (1970). *The Notebooks of Leonardo da Vinci*. New York: Dover Publications.
- Riva, C. E., Grunwald, J. E., Sinclair, S. H. and Petrig, B. L.** (1985). Blood velocity and volumetric flow rate in human retinal vessels. *Invest. Ophthalmol. Vis. Sci.* **26**, 1124-1132.
- Sato, K. and Sadamoto, T.** (2010). Different blood flow responses to dynamic exercise between internal carotid and vertebral arteries in women. *J. Appl. Physiol.* **109**, 864-869.
- Savage, V. M., Deeds, E. J. and Fontana, W.** (2008). Sizing up allometric scaling theory. *PLoS Comput. Biol.* **4**, e1000171.
- Schmid-Schönbein, H., Wells, R. and Goldstone, J.** (1969). Influence of deformability of human red cells upon blood viscosity. *Circ. Res.* **25**, 131-143.
- Seymour, R. S. and Blaylock, A. J.** (2000). The Principle of Laplace and scaling of ventricular wall stress and blood pressure in mammals and birds. *Physiol. Biochem. Zool.* **73**, 389-405.
- Seymour, R. S. and Snelling, E. P.** (2018). Calculating brain perfusion of primates. *J. Hum. Evol.* **128**, 99-102.
- Seymour, R. S., Angove, S. E., Snelling, E. P. and Cassey, P.** (2015). Scaling of cerebral blood perfusion in primates and marsupials. *J. Exp. Biol.* **218**, 2631-2640.
- Sieg, A. E., O'Conner, M. P., McNair, J. N., Grant, B. W., Agosta, S. J. and Dunham, A. E.** (2009). Mammalian metabolic allometry: do intraspecific variation, phylogeny, and regression models matter? *Am. Nat.* **174**, 720-733.
- Silvestre, J.-S., Smadja, D. M. and Lévy, B. I.** (2013). Postischemic revascularization: From cellular and molecular mechanisms to clinical applications. *Physiol. Rev.* **93**, 1743-1802.
- Smiesko, V. and Johnson, P. C.** (1993). The arterial lumen is controlled by flow-related shear stress. *News Physiol. Sci.* **8**, 34-38.
- Sokoloff, L., Mangold, R., Wechsler, R. L., Kennedy, C. and Kety, S. S.** (1955). Effect of mental arithmetic on cerebral circulation and metabolism. *J. Clin. Investig.* **34**, 1101-1108.
- Sriram, K., Intaglietta, M. and Tartakovsky, D. M.** (2014). Non-Newtonian flow of blood in arterioles: consequences for wall shear stress measurements. *Microcirculation* **21**, 628-639.
- Tan, C. O.** (2012). Defining the characteristic relationship between arterial pressure and cerebral flow. *J. Appl. Physiol.* **113**, 1194-1200.
- Tarumi, T. and Zhang, R.** (2018). Cerebral blood flow in normal aging adults: cardiovascular determinants, clinical implications, and aerobic fitness. *J. Neurochem.* **144**, 595-608.
- Tekin, E., Hunt, D., Newberry, M. G. and Savage, V. M.** (2016). Do vascular networks branch optimally or randomly across spatial scales? *PLoS Comput. Biol.* **12**, e1005223.
- Thijssen, D. H. J., Cable, N. T. and Green, D. J.** (2012). Impact of exercise training on arterial wall thickness in humans. *Clin. Sci.* **122**, 311-322.
- Townsend, R. E., Prinz, P. N. and Obrist, W. D.** (1973). Human cerebral blood flow during sleep and waking. *J. Appl. Physiol.* **35**, 620-625.
- Tronc, F., Wassef, M., Esposito, B., Henrion, D., Glagov, S. and Tedgui, A.** (1996). Role of NO in flow-induced remodeling of the rabbit common carotid artery. *Arterioscler. Thromb. Vasc. Biol.* **16**, 1256-1262.
- van Es, A. C. G. M., van der Grond, J., ten Dam, V. H., de Craen, A. J. M., Blauw, G. J., Westendorp, R. G. J., Admiraal-Behloul, F. and van Buchem, M. A.** (2010). Associations between total cerebral blood flow and age related changes of the brain. *PLoS ONE* **5**, e9825.
- Weinberg, P. D. and Ethier, C. R.** (2007). Twenty-fold difference in hemodynamic wall shear stress between murine and human aortas. *J. Biomech.* **40**, 1594-1598.
- Weisbecker, V. and Goswami, A.** (2010). Brain size, life history, and metabolism at the marsupial/placental dichotomy. *Proc. Natl. Acad. Sci. USA* **107**, 16216-16221.
- West, G. B., Brown, J. H. and Enquist, B. J.** (1997). A general model for the origin of allometric scaling laws in biology. *Science* **276**, 122-126.
- West, G. B., Brown, J. H. and Enquist, B. J.** (1999). The fourth dimension of life: fractal geometry and allometric scaling of organisms. *Science* **284**, 1677-1679.
- White, C. R. and Kearney, M. R.** (2013). Determinants of inter-specific variation in basal metabolic rate. *J. Comp. Physiol. B* **183**, 1-26.
- Wilcox, B. R., Coulter, N. A., Rackley, C. E. and Croom, R. D.** (1970). The effect of changing heart rate on blood flow, power dissipation, and resistance in the common carotid artery of man. *Ann. Surg.* **171**, 24-30.
- Willie, C. K., Tzeng, Y.-C., Fisher, J. A. and Ainslie, P. N.** (2014). Integrative regulation of human brain blood flow. *J. Physiol.* **592**, 841-859.
- Winkel, L. C., Hoogendoorn, A., Xing, R. Y., Wentzel, J. J. and Van der Heiden, K.** (2015). Animal models of surgically manipulated flow velocities to study shear stress-induced atherosclerosis. *Atherosclerosis* **241**, 100-110.
- Wolinsky, H. and Glagov, S.** (1967). A lamellar unit of aortic medial structure and function in mammals. *Circ. Res.* **20**, 99-111.
- Zamir, M. and Medeiros, J. A.** (1982). Arterial branching in man and monkey. *J. Gen. Physiol.* **79**, 353-360.
- Zamir, M., Sinclair, P. and Wonnacott, T. H.** (1992). Relation between diameter and flow in major branches of the arch of the aorta. *J. Biomech.* **25**, 1303-1310.

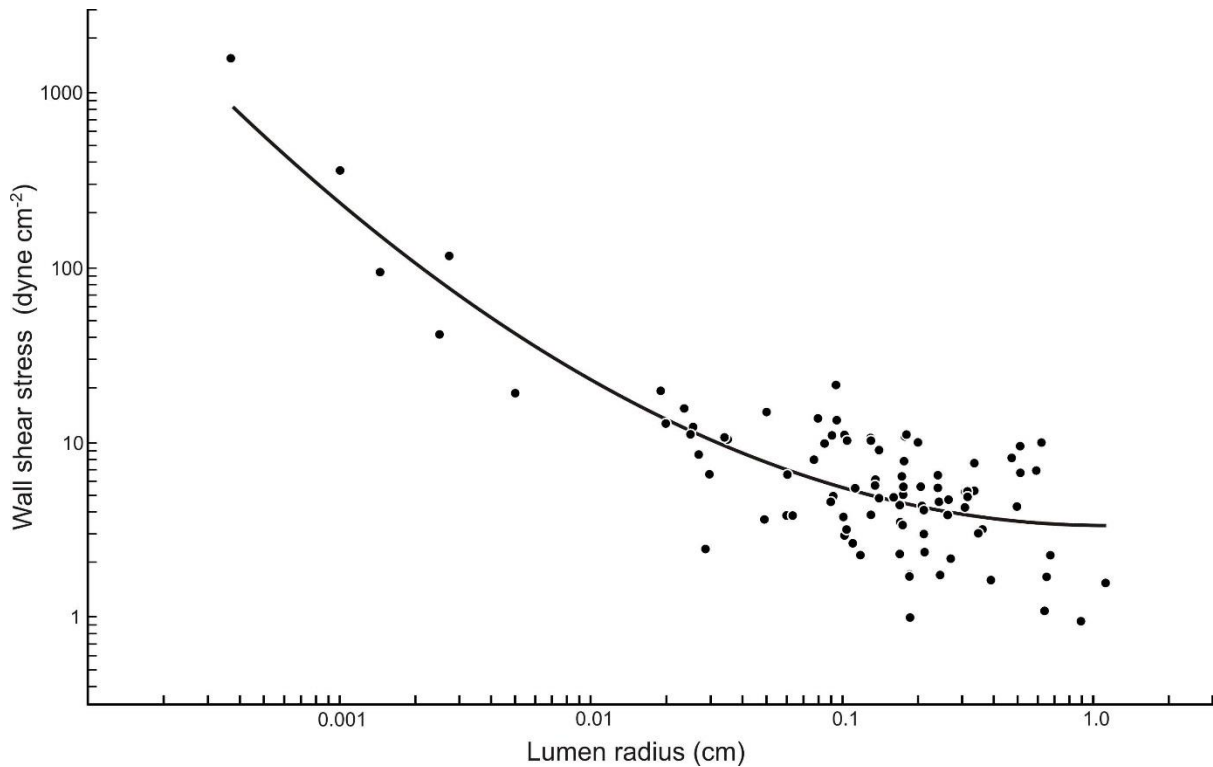


Figure S1. Relationship between log wall shear stress (τ ; dyne cm^{-2}) and log systemic arterial lumen radius (r_i ; cm) in mammals at rest, calculated from the 'modified' Poiseuille shear stress equation, $\tau = (4 \dot{Q} \eta) / (\pi r_i^n)$, where n is the derivative of the equation in Fig. 1 of the main manuscript. The equation for the polynomial mean regression line is: $\log \tau = 0.200 \log r_i^2 - 0.017 \log r_i + 0.530$ ($R^2 = 0.70$; $n = 92$).

Table S1

[Click here to Download Table S1](#)